Atmos. Chem. Phys. Discuss., 15, 4601–4625, 2015
www.atmos-chem-phys-discuss.net/15/4601/2015/
doi:10.5194/acpd-15-4601-2015

Atmospheric Chemistry and Physics Discussions

A perturbed parameter model ensemble to investigate 1991 Mt Pinatubo's initial sulfur mass emission

J.-X. Sheng[1], D. K. Weisenstein[2], B.-P. Luo[1], E. Rozanov[1,3], F. Arfeuille[4,*], and T. Peter[1]

[1]Institute for Atmospheric and Climate Science, ETH Zurich, Zurich, Switzerland
[2]School of Engineering and Applied Science, Harvard University, Cambridge, MA, USA
[3]Physical-Meteorological Observatory/World Radiation Center, Davos, Switzerland
[4]Oeschger Centre for Climate Change Research and Institute of Geography, University of Bern, Bern, Switzerland
[*]now at: Empa, Swiss Federal Laboratories for Materials Testing and Research, Dübendorf, Switzerland

Received: 8 December 2014 – Accepted: 5 January 2015 – Published: 18 February 2015

Correspondence to: J.-X. Sheng (sh3ngj@gmail.com)

Published by Copernicus Publications on behalf of the European Geosciences Union.

Abstract

We have performed more than 300 atmospheric simulations of the 1991 Pinatubo eruption using the AER 2-D sulfate aerosol model to optimize the initial sulfur mass injection as function of altitude, which in previous modeling studies has often been chosen in an ad hoc manner (e.g., by applying a rectangular-shaped emission profile). Our simulations are generated by varying a 4-parameter vertical mass distribution, which is determined by a total injection mass and a skew-normal distribution function. Our results suggest that (a) the initial mass loading of the Pinatubo eruption is approximately 14 Mt of SO_2, (b) the injection vertical distribution is strongly skewed towards the lower stratosphere, leading to a peak mass sulfur injection at 19–22 km. The optimized distribution largely improves the previously found overestimates in modeled extinctions in comparison with SAGE II solar occultation measurements.

1 Introduction

The eruption of Mt Pinatubo on 15 June 1991 injected large amounts of sulfur dioxide into the stratosphere. It perturbed the radiative, dynamical and chemical processes in the Earth atmosphere (McCormick et al., 1995) and caused a global surface cooling of approximately 0.5 K (Dutton and Christy, 1992). The Pinatubo eruption serves as a useful analogue for geoengineering via injection of sulfur-containing gases into the stratosphere (Crutzen, 2006; Robock et al., 2013). Therefore, modeling volcanic eruptions advances our knowledge not only of the eruptions themselves on weather and climate, but also potential impacts of stratospheric sulfate geoengineering.

The uncertainties in determining the initial total mass and altitude distribution of SO_2 released by Pinatubo remain high. Stowe et al. (1992) deduced a mass of 13.6 megatons of SO_2 based on the aerosol optical thickness observed by the Advanced Very High Resolution Radiometer (AVHRR). By analyzing SO_2 absorption measurements from the Total Ozone Mapping Spectrometer (TOMS) satellite instrument, Bluth et al.

ACPD
15, 4601–4625, 2015

(1992) estimated an initial mass loading of approximately 20 Mt of SO_2. This study was later reevaluated by Krueger et al. (1995), who determined a range of 14–28 Mt emitted by Pinatubo, given the large retrieval uncertainties associated with TOMS. Later, Guo et al. (2004) constrained this range to 14–22 Mt of SO_2. Besides the total emitted mass, the altitude distribution of the SO_2 emission is also not well constrained. The only available measurements with vertical resolution of SO_2 in the stratosphere during the Pinatubo period have been made by the Microwave Limb Sounder (MLS) in September 1991 (Read et al., 1993), which unfortunately only started its mission three months after the eruption. Given the lack of measurements in the period immediately following the Pinatubo eruption, modeling studies of Pinatubo (e.g., Weisenstein et al., 1997; Timmreck et al., 1999; SPARC, 2006; Heckendorn et al., 2009; Niemeier et al., 2009; Toohey et al., 2011; Aquila et al., 2012; English et al., 2013; Dhomse et al., 2014) have employed very different mass loadings, emission altitudes and vertical mass distributions, which leads to biases in the local heating and consequently in the dynamical responses and time evolution of the stratospheric aerosol burden. These uncertainties make it difficult to accurately simulate the Pinatubo eruption in addition to model-specific artifacts.

Here, we attempt to provide a solution to the problems outlined above. We use the AER 2-D size-bin resolving (also called sectional or spectral) sulfate aerosol model (Weisenstein et al., 1997), which participated in a recent international aerosol assessment (SPARC, 2006), and was one of the best-performing stratospheric aerosol models. We present results from more than 300 atmospheric simulations of the Pinatubo eruption based on different combinations of four emission parameters, namely the total SO_2 mass and a 3-parameter skew-normal distribution of SO_2 as function of altitude. We calculate aerosol extinctions from all of the simulations and compare them with Stratospheric Aerosol and Gas Experiment II (SAGE II) measurements (Thomason et al., 1997, 2008). Such a head-on approach is currently impossible for global 3-D models due to computational expenses. The purpose of this work is to provide a universal emission scenario for global 3-D model simulations. To this end we opti-

ACPD
15, 4601–4625, 2015

mize the emission parameters such that the resulting SO_2 plume, aerosol size distributions, aerosol burdens and extinctions match balloon-borne, satellite and lidar measurements. In Sect. 2 we describe the 2-D model and the experimental design of our Pinatubo simulations. Section 3 compares the Pinatubo simulations with the observations, and conclusions follow in Sect. 4.

2 Method

2.1 AER 2-D sulfate aerosol model

The AER 2-D sulfate aerosol model participated in a recent international aerosol assessment (SPARC, 2006), in which it was compared with satellite, ground lidar and balloon measurements, as well as with other 2-D and 3-D aerosol models, and subsequently recognized as one of the best existing stratospheric aerosol models. The model represents sulfuric acid aerosols (H_2SO_4/H_2O) on the global domain from the surface to about 60 km with approximately 9.5° horizontal and 1.2 km vertical resolution. The model is driven by year-by-year wind fields and temperature from Fleming et al. (1999), which were derived from observed ozone, water vapor, zonal wind, temperature, planetary waves, and quasi-biennial oscillation (QBO). The model chemistry includes the sulfate precursor gases carbonyl sulfide (OCS), sulfur dioxide (SO_2), sulfur trioxide (SO_3), sulfuric acid (H_2SO_4), dimethyl sulfide (DMS), carbon disulfide (CS_2), hydrogen sulfide (H_2S) and methyl sulfonic acid (MSA). The model uses pre-calculated values of OH and other oxidants from Weisenstein et al. (1996). Photodissociation and chemical reactions are listed in Weisenstein et al. (1997) and their rates are updated to Sander et al. (2011). The particle distribution is resolved by 40 size bins spanning wet radii from 0.39 nm to 3.2 µm by volume doubling. Such a sectional approach was proven to be more accurate in representing aerosol mass/extinctions compared to prescribed unimodal or multimodal lognormal distributions (Weisenstein et al., 2007). The sulfuric acid aerosols are treated as liquid binary solution droplets. Their exact com-

ACPD
15, 4601–4625, 2015

position is directly derived from the surrounding temperature and humidity according to Tabazadeh et al. (1997). Microphysical processes in the model include homogeneous nucleation, condensation/evaporation, coagulation, sedimentation, as well as tropospheric rainout/washout. These processes determine the evolution of the aerosol concentration in each size bin, thus the entire particle size distribution. Operator splitting methods are used in the model with a time step of one hour for transport, chemistry, and microphysics, and 3 min substeps for the microphysical processes that exchange gas-phase H_2SO_4 with condensed phase, and 15 min substeps for the coagulation process. For more detailed descriptions of chemistry and microphysics in the model we refer to Weisenstein et al. (1997, 2007).

2.2 Coupled 3-D aerosol-chemistry-climate model

We employ the couple aerosol-chemistry-climate model SOCOL-AER (Sheng et al., 2014) in order to verify the consistency between a 2-D model forced with observed dynamics and a 3-D free-running model. SOCOL-AER couples the size resolved AER 2-D microphysical model into the chemistry-climate model SOCOL (Stenke et al., 2013) with interactive aerosol radiative forcing. In this study we use the T31 horizontal resolution (3.75° × 3.75°) and 39 vertical levels (from surface to 0.01 hPa) with operator splitting approaches in time: transport is calculated every 15 min, whereas chemistry, microphysics and radiation are calculated every two hours with 40 substeps (3 min) for the microphysics. This model has been well validated by comparing calculations with sulfur-containing gases, aerosol extinctions at different wavelength channels (from 525 nm to 5.26 µm), and aerosol size distributions from satellite and in situ observations. It has been used to study the global atmospheric sulfur budget under volcanically quiescent conditions and moderate volcanic eruptions such as the 2011 Nabro eruption. A detailed description of SOCOL-AER is presented by Sheng et al. (2014).

ACPD
15, 4601–4625, 2015

2.3 Experiments

We have simulated the Pinatubo-like eruption by injecting SO_2 directly into the stratosphere. In the 2-D model, the injection is immediately mixed zonally, and takes place into the latitude band 5° S–14° N, which is an approximation to the observed rapid zonal transport of the SO_2 cloud derived from satellite measurements (Bluth et al., 1992; Guo et al., 2004). The lack of zonal resolution is clearly a deficiency of our approach, but since SO_2 removal/conversion rate (e-folding time) is sufficiently slow ($\tau \sim 25$ days) and the zonal transport around the globe sufficiently fast ($\tau \sim 20$ days) (Guo et al., 2004), a zonal-mean description is a reasonable approximation. Also, the spaceborne aerosol data are typically provided as zonal averages. We examined three cases of total mass, namely 14, 17 and 20 Mt of SO_2. The injection height extends from near the tropical tropopause (17 km) to 30 km. The vertical mass distribution is then represented by $M_{\text{tot}}F(z)$ where M_{tot} is the SO_2 mass magnitude in units of megaton (Mt) and $F(z) = f(z)/\int_{z_{\min}=17}^{z_{\max}=30} f(x)\,\mathrm{d}x$ (in km^{-1}) is a vertical distribution function of altitude $z \in [17, 30\,\mathrm{km}]$ with a skew-normal distribution $f(z)$ given by (Azzalini, 2005)

$$f(z) = \frac{2}{\sqrt{2\pi}\sigma} e^{-\frac{(z-\mu)^2}{2\sigma^2}} \int_{-\infty}^{\alpha\frac{z-\mu}{\sigma}} \frac{1}{\sqrt{2\pi}} e^{-\frac{x^2}{2}}\,\mathrm{d}x.$$

Figure 1 shows a few examples of $F(z)$. The location parameter μ depends on available model levels and determines the altitude where the maximum of the emitted SO_2 cloud is located when there is no skewness. The skewness or asymmetry of the curve increases when $|\alpha|$ increases and vanishes when $\alpha = 0$ (normal distribution). A negative α drives the location of the maximum SO_2 emission to lower altitudes, while a positive α to higher altitudes. The scale parameter σ indicates how much dispersion takes place near the maximum, that is, it determines the width or SD of the asymmetric bell-shaped curve.

ACPD
15, 4601–4625, 2015

The four parameters M_{tot}, μ, σ and α enable representation of a substantial space of SO_2 distributions, whose evolution is computed forward in time (taking into account the transport and comprehensive chemical and microphysical processes), in order to compare with the satellite extinction data. We simulate the following cases in detail:

$$M_{tot} \in \{14, 17, 20\,\text{Mt}\},$$
$$\mu \in \{16.79\,\text{km} + n \times 1.16\,\text{km}, \quad n = 0...11\},$$
$$\sigma \in \{2, 3, 4\,\text{km}\},$$
$$\alpha \in \{-2, -1, 0\},$$

which results in 324 different scenarios. The choice of the boundaries for this set of scenarios is already based on exploratory simulations. For example, based on the results of our 2-D model, it does not make sense to consider total masses $M_{tot} > 20$ Mt, since no choice of the other three parameters would allow to reconcile the model results with the observations. Similarly, skewness $\alpha > 0$ can lead to more biased model results, because the skew towards higher altitudes cannot be offset by lower M_{tot}. In addition to the above 324 simulations, we consider another two scenarios, which are adopted in modeling studies of Pinatubo: (1) Box14Mt has a uniform ("Box") profile, which is similar to Dhomse et al. (2014) and the simulation "CONTROL_HIGH" in Aquila et al. (2012), injecting the SO_2 mass homogeneously along altitudes (shown in Fig. 1), (2) SPARC20Mt is the reproduction of the Pinatubo simulation conducted in SPARC (2006), which injects 20 Mt of SO_2 and has a vertical profile "SPARC" shown in Fig. 1.

A selected list from the 326 simulations is summarized in Table 1, in which the specific choice of the four parameters for each scenario is provided. The score and ranking of these scenarios are discussed later in the text.

Given the limitation of the 2-D approach, we further perform two 3-D Pinatubo-like simulations (R001 3-D and R149 3-D at the bottom of Table 1) using the coupled aerosol-chemistry-climate model SOCOL-AER (Sheng et al., 2014) to check the consistency between 2-D and 3-D approaches. Note that the location parameters used in

ACPD
15, 4601–4625, 2015

the 3-D runs differ slightly from the corresponding 2-D runs (i.e. R001 and R149) due to different vertical model levels between the two models.

3 Results and discussions

We compare our results with SO_2 vertical profiles measured by the Microwave Limb Sounder (MLS) onboard the Upper Atmosphere Research Satellite (UARS) between 10° S–0° in September 1991 (Read et al., 1993), the optical particle counter (OPC) measurements operated above Laramie, Wyoming (Deshler et al., 2003; Deshler, 2008), the global aerosol burden derived from the High-resolution Infrared Radiation Sounder (HIRS) (Baran and Foot, 1994) and from Stratospheric Aerosol and Gas Experiment II (SAGE II) using the 4λ method (SAGE-4λ) (Arfeuille et al., 2013), as well as aerosol extinctions measured by SAGE II (Thomason et al., 1997, 2008).

Metrics and data sets. To determine an optimal set of the emission parameters, we define four metrics (ScoreSO_2, ScoreBurden, ScoreOPC and ScoreExt) based on these four measurements sets described above, and rank all of our 324 simulations by a weighted score (ScoreWt) of the four metrics (see Table 1). ScoreSO_2 is calculated as the relative l^2-norm (Euclidean norm) error with respect to the MLS measurements, whose negative values are set to zero in the calculation. ScoreBurden is the average of the relative l^2-norm errors with respect to HIRS (July–December 1991) and SAGE-4λ (January 1992–December 1993). ScoreOPC is evaluated by the relative l^2-norm errors (in space) with respect to the OPC measurements for four particle size channels ($r > 0.01\,\mu m$, $r > 0.15\,\mu m$, $r > 0.25\,\mu m$ and $r > 0.5\,\mu m$), and then averaged over time (from October 1991 to December 1992). ScoreExt is evaluated by the relative l^2-norm error (in space) with respect to gap-filled SAGE II v7.0, and then averaged over time (from January 1992 to December 1993). The overall score ScoreWt is weighted as follows: 16.7 % of the SO_2 score (ScoreSO_2), 16.7 % of the OPC score (ScoreOPC), 33.3 % of the global burden score (ScoreBurden), and 33.3 % of the aerosol extinction score (ScoreExt). The choice of the weighting is discussed below.

ACPD
15, 4601–4625, 2015

MLS detected residual SO_2 in the stratosphere after approximately 100 days after the eruption. The uncertainty of ScoreSO_2 is likely larger than ScoreBurden and ScoreExt due to short lifetime of SO_2 and uncertain OH fields. Assuming an uncertainty in OH fields of 10 % (e.g., Prinn et al., 2005) translates into an uncertainty of 30 % in SO_2 at ~ 90 days after the eruption. Moreover, ScoreOPC has also less weight than ScoreBurden and ScoreExt because of the small temporal and spatial sample size of the ballon-borne OPC measurements, which are not conducted very frequently (a maximum of two measurements per month after the Pinatubo eruption) and located only above Laramie. In contrast, SAGE II, as an occultation instrument, becomes very reliable when the stratosphere starts to be sufficiently transparent. The measurement uncertainty is generally better than ~ 20 % for 525 nm wavelength and ~ 10 % for 1020 nm (see Fig. 4.1 in SPARC, 2006). Therefore, ScoreExt is weighted as one third for 525 nm and two thirds for 1020 nm. Finally, ScoreBurden uses the HIRS-derived data up to month 12 and the SAGE-derived data afterwards. During the first year after the Pinatubo eruption, the SAGE II instrument was largely saturated in the tropical region (Russell et al., 1996; Thomason et al., 1997; SPARC, 2006; Arfeuille et al., 2013), and therefore the aerosol mass retrieved from SAGE II during this period very likely underestimates the initial loading significantly. The SAGE-4λ data set corrects for this deficiency by filling observational gaps by means of Lidar data. However, Lidar-derived extinctions are generally lower than SAGE II below 21 km (SPARC, 2006), and are not located in the equatorial region (see Fig. 3.7 in SPARC, 2006), where maximum mass loadings are expected. Therefore, SAGE II gap-filled data probably remain as a lower limit after the eruption. Conversely, HIRS measurements represent an upper limit since they account for the entire aerosol column including the troposphere. This may explain the considerable difference between SAGE II and HIRS during the first year after Pinatubo (see Fig. 3). After this period, HIRS tends to be noisy due to its lack of sensitivity at high latitudes where there is a contribution from errors in the background signal (Baran and Foot, 1994). In contrast, SAGE II, as an occultation instrument, becomes more reliable when the stratosphere starts to be sufficiently transparent. Therefore,

ACPD
15, 4601–4625, 2015

ScoreBurden uses the HIRS-derived data up to month 12 and the SAGE-derived data afterwards, with an overall uncertainty of 20 %.

Scoring table. Table 1 shows the scores of selected scenarios, sorted according to the weighted rank ("RankWt" in the next to last column). The best scenarios (RankWt ≤ 15) reveal that the total injection mass (M_{tot}) is 14 Mt of SO_2, 70–80 % of which is below 24 km, and its maximum is likely between 19–22 km with 3–4 km width (scale parameter σ). Location parameters μ larger than 22 km are generally skewed towards a lower altitude (negative α). These sort of vertical profiles provide a range for the parameters of the optimal vertical distribution: $\mu = 20.66 \pm 1.79$ km, $\sigma = 3.33 \pm 0.72$ km and $\alpha = -0.8 \mp 0.77$. Two examples (scenarios R001 and R010 marked in Table 1) are shown in Fig. 1. The worst scenarios (RankWt ≥ 317) in Table 1 are those with 20 Mt SO_2 injection mass and highest location parameters ($\mu = 29.55$ km). The scenarios such as Box14Mt and R149 rank much more poorly than the optimal scenarios, although their injection mass is the same, because their vertical profiles (shown in Fig. 1) inject over 50 % mass above 23–24 km. The scenario R034 has the same vertical profile as R001, but more emitted mass (17 Mt SO_2), leading to poorer ranks in the aerosol burden and extinctions. The scenario SPARC20Mt ranks at 211 in Table 1, although its vertical profile is close to the optimal scenarios (about 10–20 % more mass above 23 km). This implies that emitting 17 or 20 Mt SO_2 is very likely an overestimation.

The optimal vertical profiles found in Table 1 are generally consistent with the earlier volcanic plume studies of Fero et al. (2009) and Herzog and Graf (2010). Fero et al. (2009) showed that the SO_2 plume from the 1991 Pinatubo eruption originated at an altitude of ~ 25 km near the source and descended to an altitude of ~ 22 km as the plume moved across the Indian Ocean. Herzog and Graf (2010) suggested that initially SO_2 from a co-ignimbrite eruption (such as Pinatubo) that was forced over a large area, may reach above 30 km but the majority of SO_2 would then collapse or sink back to its neutral buoyancy height (15–22 km) (see Fig. 1 in their paper).

We choose seven scenarios (R001, R034, R149, Box14Mt, SPARC20Mt, R001 3-D and R149 3-D) to be discussed in detail. R001 represents the optimal scenario. In

ACPD
15, 4601–4625, 2015

comparison, R034, R149 and Box14Mt are in the center span of the ranking field: R034 has the same vertical profile as R001, but injects larger sulfur mass (17 Mt SO_2); R149 and Box14Mt (with Rank 94) inject the same sulfur mass as in R001, but use different vertical profiles (maximum injection mass of R149 is located at 26 km). SPARC20Mt (with Rank 216) turns out to be a bad representation, which reproduces the previous simulation conducted in SPARC (2006). The two 3-D scenarios R001 3-D and R149 3-D correspond to the 2-D scenarios R001 and R149, respectively. The scores of the 3-D simulations are similar to the corresponding 2-D simulations.

Matching SO_2. Figure 2 shows the comparison of modeled SO_2 with MLS measurements three months after the eruption. The scenario R001 captures the measured SO_2 profile, and only underestimates the measured maximum SO_2 mixing ratio near 26 km by about 20 %. SO_2 modeled by R034 shows excellent agreement (within 7 %) with MLS measurement. Box14Mt and R149 fail to match the observed profile, and SPARC20Mt shows better agreement with the observations under 28 km, but nevertheless largely overestimates the observations above. The common feature of R149, Box14Mt and SPARC20Mt is that their initial vertical distributions release much more SO_2 above 24 km compared to R001, which is skewed towards lower altitudes, therefore retaining more than 90 % of emitted SO_2 below 24 km (Fig. 1). SO_2 distributions simulated by the two 3-D simulations (dashed curves in Fig. 2) are similar to the corresponding AER 2-D simulations, though SOCOL-AER predicts a lower maximum value and more readily distributes SO_2 to higher altitudes, reflecting differences in OH and transport between the two models.

Matching the burden. Figure 3 shows the evolution of the simulated stratospheric aerosol burden (integrated above the tropopause) in units of teragram of H_2SO_4/H_2O droplet total mass compared to the aerosol mass derived from HIRS (Baran and Foot, 1994), and SAGE II using the 4λ method (Arfeuille et al., 2013). In Fig. 3, R001 matches the HIRS-derived maximum aerosol burden during the first few months after the eruption, and after month 14 agrees with the SAGE-derived burden (mostly within 20 %). In contrast, SPARC20Mt reaches a maximum burden of 32 Mt of H_2SO_4/H_2O, which

ACPD
15, 4601–4625, 2015

is ∼ 50 % more than the 21 Mt derived from HIRS. R034 emits 17 Mt of SO_2 using the same vertical profile as R001, and peaks at 25 Mt of aerosol mass, about ∼ 30 % more than HIRS, whereas the uncertainty of HIRS is about 10 % (Baran and Foot, 1994). This means that the initial mass loading of 17 or 20 Mt of SO_2 into the stratosphere is apparently too high. Different vertical profiles using 14 Mt of SO_2 show a high sensitivity in the evolution of the aerosol burden. R149 and Box14 Mt inject about 60 and 40 % of their sulfur mass above 24 km, respectively, and lead to a greater maximum aerosol burden than R001. R149 has even a slightly larger maximum aerosol burden than R034, even though R034 has the larger initial SO_2 mass loading. This is likely due to the fact that above 24 km the mean age-of-air and the residence time of sedimenting aerosol are greater than in the lower stratosphere, where most of the sulfur mass of R001 and R034 is located. The results of "R001 3-D" using the coupled aerosol-chemistry-climate model SOCOL-AER is consistent (mostly within 10 %) with the AER 2-D simulation R001. In contrast, the consistency between R149 and "R149 3-D" is less satisfactory. The maximum aerosol burden simulated by "R149 3-D" is within 10 % of R149, but the e-folding time of the aerosol burden in the 3-D simulation ("R149 3-D") is significantly faster (13 vs. 15 months) than in the 2-D simulation (R149), indicating that in addition to the initial mass loading and microphysics also the model dynamics plays an important role in the decay of the volcanic aerosols. This difference between R149 (AER) and "R149 3-D" (SOCOL-AER) is possibly due to an insufficient rate of exchange of air between the troposphere and stratosphere in the AER 2-D model (Weisenstein et al., 1997) and/or a faster Brewer–Dobson circulation in the middle stratosphere using the free-running 3-D SOCOL-AER. Indeed, SOCOL-AER has a too fast tape recorder signal, which is a measure of the Brewer–Dobson circulation (Stenke et al., 2013).

Matching particle size distributions. Figure 4 shows comparisons between the optical particle counter (OPC) measurements operated above Laramie (Deshler et al., 2003; Deshler, 2008) and model-calculated cumulative particle number concentrations in October and December 1991 for two size channels ($r > 0.15\,\mu m$ and $r > 0.5\,\mu m$). Below 23 km, R001 reasonably matches the observations for $r > 0.15\,\mu m$, but less satisfac-

ACPD
15, 4601–4625, 2015

torily for $r > 0.5\,\mu m$. R034 predicts slightly higher number concentrations than R001 due to its larger initial mass loading (17 Mt SO_2), but shows in general similar results to R001. In contrast, the calculations from R149, Box14Mt and SPARC20Mt differ significantly from R001. Above 23 km, these three scenarios further overestimate the observations than R001 because their initial injection profiles release more SO_2 above 23 km compared to R001. Below 23 km, R149 substantially underestimates the observations in October 1991 as its injected mass is mainly situated between 23–27 km, while Box14Mt shows better agreement with the observations ($r > 0.5\,\mu m$) below 18 km than R001, but largely underestimates the maximum near 21 km. SPARC20Mt is similar to R001 below 20 km since its initial mass loading (20 Mt SO_2) compensates for the deficiency of its vertical mass injection profile in the lower stratosphere. The calculations from SOCOL-AER are generally consistent with the corresponding 2-D calculations (R001 and R149). SOCOL-AER produces higher number concentration in October 1991 compared to the AER 2-D model. In December 1991 this difference between the 2-D and 3-D simulations shrinks, and "R001 3-D" further improves the agreement with the OPC measurements below 18 km for $r > 0.5\,\mu m$.

Matching extinctions. We compare the modeled 1020 nm extinctions with the gap-filled SAGE II version 7.0 (Fig. 5). SAGE II data points with horizontal bars are actual SAGE II measurements and denote natural variabilities, while data points without bars are gap-filled from lidar ground stations, which have a higher uncertainty (SPARC, 2006). Figure 5 shows comparisons in January (upper panel) and July (lower pannel) 1992 for five latitude bands from left to right: 50–40° S, 30–20° S, 5° S–5° N, 20–30° N and 40–50° N.

In January 1992, all the simulations reproduce aerosol extinctions reasonably near 20 km (mostly within 50–100 % of observed aerosol extinctions). The calculations with R001 agree better with observed aerosol extinctions compared to the other 2-D simulations, particularly above 24 km. R034 is generally 10–20 % larger than R001 due to its higher initial mass loading, although it has the same vertical profile as R001. SPARC20Mt has even larger values than R034 due to a 20 Mt of SO_2 mass loading.

ACPD
15, 4601–4625, 2015

Box14Mt and R149 largely overestimate the observed extinctions above 24 km. The 3-D simulation "R001 3-D" is superior to all the 2-D simulations, while "R149 3-D" performs worse than the 2-D simulations R001 and R034. Likewise, in June 1992, R001 also does a better job than other 2-D simulations. The two 3-D simulations "R001 3-D" and "R149 3-D" are now both superior to all 2-D model results, although the differences between them start to shrink as the their aerosol burdens are now within 10 % from each other. Overall, the calculations of SPARC20Mt, Box14Mt, R034 and R149 display a common deficiency, as they tend to overestimate aerosol extinctions in high altitudes above 24 km. Excessive initial mass loading (as in SPARC20Mt or R034) is one of the reasons. However, the shape of the initial mass vertical profiles appears to be at least as important as the initial mass loading. Box14Mt has 30 % less total mass loading than SPARC20Mt, but it shows even higher extinctions in high altitudes because it has 40 % of its mass injected above 24 km, while SPARC20Mt has only about 20 % of its mass there.

4 Conclusions

We have conducted over 300 Pinatubo-like simulations based on variations of four parameters of initial total SO_2 mass and altitude distribution. These parameters control the temporal and spatial evolution of stratospheric aerosols in the years following the Pinatubo eruption. The altitude distribution of SO_2 injection is represented by a skew-normal distribution. Our simulations suggest that Pinatubo injected less than 17 Mt of SO_2 into the stratosphere and that good agreement can be reached with a 14 Mt injection, 80 % of which was injected below 24 km with the maximum located between 19–22 km. This reproduces HIRS and SAGE II-based estimates of the evolution of total stratospheric aerosol burden. Furthermore, this largely improves the previous overestimates in modeled extinctions at high altitudes when comparing to SAGE II gap-filled measurements SPARC (2006), and realistically simulates aerosol extinctions in the lower stratosphere. We have defined an optimal set of the emission parameters such

ACPD
15, 4601–4625, 2015

that the resulting burdens and extinctions match satellite and lidar measurements, and reduce the uncertainties in modeling the initial sulfur mass loading of Pinabuto.

Acknowledgements. This work was stimulated by the "Assessment of Stratospheric Aerosol Properties (ASAP)", a previous activity of SPARC (Stratosphere–troposphere Processes and their Role in Climate). We thank Laura Revell for useful comments. We thank Jason English and Anthony Baran for helpful discussion on HIRS measurements. Also thanks to Andrew Gettelman for useful suggestions on our work. We are particularly grateful to Mian Chin for valuable comments which helped to improve the manuscript. This work was supported by the Swiss National Science Foundation under the grant 200021-130478 (IASSA).

References

Aquila, V., Oman, L. D., Stolarski, R. S., Colarco, P. R., and Newman, P. A.: Dispersion of the volcanic sulfate cloud from a Mount Pinatubo–like eruption, J. Geophys. Res.-Atmos., 117, D06216, doi:10.1029/2011JD016968, 2012. 4603, 4607

Arfeuille, F., Luo, B. P., Heckendorn, P., Weisenstein, D., Sheng, J. X., Rozanov, E., Schraner, M., Brönnimann, S., Thomason, L. W., and Peter, T.: Modeling the stratospheric warming following the Mt. Pinatubo eruption: uncertainties in aerosol extinctions, Atmos. Chem. Phys., 13, 11221–11234, doi:10.5194/acp-13-11221-2013, 2013. 4608, 4609, 4611, 4623

Azzalini, A.: The skew-normal distribution and related multivariate families, Scand. J. Stat., 32, 159–188, doi:10.1111/j.1467-9469.2005.00426.x, 2005. 4606

Baran, A. J. and Foot, J. S.: New application of the operational sounder HIRS in determining a climatology of sulphuric acid aerosol from the Pinatubo eruption, J. Geophys. Res.-Atmos., 99, 25673–25679, doi:10.1029/94JD02044, 1994. 4608, 4609, 4611, 4612, 4623

Bluth, G. J. S., Doiron, S. D., Schnetzler, C. C., Krueger, A. J., and Walter, L. S.: Global tracking of the SO_2 clouds from the June, 1991 Mount Pinatubo eruptions, Geophys. Res. Lett., 19, 151–154, doi:10.1029/91GL02792, 1992. 4602, 4606

Crutzen, P. J.: Albedo enhancement by stratospheric sulfur injections: a contribution to resolve a policy dilemma?, Climatic Change, 77, 211–220, doi:10.1007/s10584-006-9101-y, 2006. 4602

ACPD
15, 4601–4625, 2015

Deshler, T.: A review of global stratospheric aerosol: measurements, importance, life cycle, and local stratospheric aerosol, Atmos. Res., 90, 223–232, doi:10.1016/j.atmosres.2008.03.016, 2008. 4608, 4612, 4624

Deshler, T., Hervig, M. E., Hofmann, D. J., Rosen, J. M., and Liley, J. B.: Thirty years of in situ stratospheric aerosol size distribution measurements from Laramie, Wyoming (41°N), using balloon-borne instruments, J. Geophys. Res.-Atmos., 108, 4167, doi:10.1029/2002JD002514, 2003. 4608, 4612, 4624

Dhomse, S. S., Emmerson, K. M., Mann, G. W., Bellouin, N., Carslaw, K. S., Chipperfield, M. P., Hommel, R., Abraham, N. L., Telford, P., Braesicke, P., Dalvi, M., Johnson, C. E., O'Connor, F., Morgenstern, O., Pyle, J. A., Deshler, T., Zawodny, J. M., and Thomason, L. W.: Aerosol microphysics simulations of the Mt. Pinatubo eruption with the UM-UKCA composition-climate model, Atmos. Chem. Phys., 14, 11221–11246, doi:10.5194/acp-14-11221-2014, 2014. 4603, 4607

Dutton, E. G. and Christy, J. R.: Solar radiative forcing at selected locations and evidence for global lower tropospheric cooling following the eruptions of El Chichón and Pinatubo, Geophys. Res. Lett., 19, 2313–2316, doi:10.1029/92GL02495, 1992. 4602

English, J. M., Toon, O. B., and Mills, M. J.: Microphysical simulations of large volcanic eruptions: Pinatubo and Toba, J. Geophys. Res.-Atmos., 118, 1880–1895, doi:10.1002/jgrd.50196, 2013. 4603

Fero, J., Carey, S. N., and Merrill, J. T.: Simulating the dispersal of tephra from the 1991 Pinatubo eruption: implications for the formation of widespread ash layers, J. Volcanol. Geoth. Res., 186, 120–131, doi:10.1016/j.jvolgeores.2009.03.011, 2009. 4610

Fleming, E. L., Jackman, C. H., Stolarski, R. S., and Considine, D. B.: Simulation of stratospheric tracers using an improved empirically based two-dimensional model transport formulation, J. Geophys. Res.-Atmos., 104, 23911–23934, doi:10.1029/1999JD900332, 1999. 4604

Guo, S., Bluth, G. J. S., Rose, W. I., Watson, I. M., and Prata, A. J.: Re-evaluation of SO_2 release of the 15 June 1991 Pinatubo eruption using ultraviolet and infrared satellite sensors, Geochem. Geophy. Geosy., 5, Q04001, doi:10.1029/2003GC000654, 2004. 4603, 4606

Heckendorn, P., Weisenstein, D., Fueglistaler, S., Luo, B. P., Rozanov, E., Schraner, M., Thomason, L. W., and Peter, T.: The impact of geoengineering aerosols on stratospheric temperature and ozone, Environ. Res. Lett., 4, 045108, doi:10.1088/1748-9326/4/4/045108, 2009. 4603

ACPD
15, 4601–4625, 2015

Herzog, M. and Graf, H.-F.: Applying the three-dimensional model ATHAM to volcanic plumes: dynamic of large co-ignimbrite eruptions and associated injection heights for volcanic gases, Geophys. Res. Lett., 37, L19807, doi:10.1029/2010GL044986, 2010. 4610

Krueger, A. J., Walter, L. S., Bhartia, P. K., Schnetzler, C. C., Krotkov, N. A., Sprod, I., and Bluth, G. J. S.: Volcanic sulfur dioxide measurements from the total ozone mapping spectrometer instruments, J. Geophys. Res.-Atmos., 100, 14057–14076, doi:10.1029/95JD01222, 1995. 4603

McCormick, M. P., Thomason, L. W., and Trepte, C. R.: Atmospheric effects of the Mt Pinatubo eruption, Nature, 373, 399–404, doi:10.1038/373399a0, 1995. 4602

Niemeier, U., Timmreck, C., Graf, H.-F., Kinne, S., Rast, S., and Self, S.: Initial fate of fine ash and sulfur from large volcanic eruptions, Atmos. Chem. Phys., 9, 9043–9057, doi:10.5194/acp-9-9043-2009, 2009. 4603

Prinn, R. G., Huang, J., Weiss, R. F., Cunnold, D. M., Fraser, P. J., Simmonds, P. G., McCulloch, A., Harth, C., Reimann, S., Salameh, P., O'Doherty, S., Wang, R. H. J., Porter, L. W., Miller, B. R., and Krummel, P. B.: Evidence for variability of atmospheric hydroxyl radicals over the past quarter century, Geophys. Res. Lett., 32, L07809, doi:10.1029/2004GL022228, 2005. 4609

Read, W. G., Froidevaux, L., and Waters, J. W.: Microwave limb sounder measurement of stratospheric SO_2 from the Mt. Pinatubo Volcano, Geophys. Res. Lett., 20, 1299–1302, doi:10.1029/93GL00831, 1993. 4603, 4608, 4622

Robock, A., MacMartin, D. G., Duren, R., and Christensen, M. W.: Studying geoengineering with natural and anthropogenic analogs, Climatic Change, 121, 445–458, doi:10.1007/s10584-013-0777-5, 2013. 4602

Russell, P. B., Livingston, J. M., Pueschel, R. F., Bauman, J. J., Pollack, J. B., Brooks, S. L., Hamill, P., Thomason, L. W., Stowe, L. L., Deshler, T., Dutton, E. G., and Bergstrom, R. W.: Global to microscale evolution of the Pinatubo volcanic aerosol derived from diverse measurements and analyses, J. Geophys. Res.-Atmos., 101, 18745–18763, doi:10.1029/96JD01162, 1996. 4609

Sander, S., Abbatt, J., Barker, J., Burkholder, J., Friedl, R., Golden, D., Huie, R., Kolb, C., Kurylo, M., Moortgat, G., Orkin, V., and Wine, P.: Chemical Kinetics and Photochemical Data for Use in Atmospheric Studies, Evaluation No. 17, JPL Publication 10-6, Jet Propulsion Laboratory, Pasadena, 2011. 4604

ACPD
15, 4601–4625, 2015

Sheng, J.-X., Weisenstein, D. K., Luo, B.-P., Rozanov, E., Stenke, A., Anet, J., Bingemer, H., and Peter, T.: Global atmospheric sulfur budget under volcanically quiescent conditions: aerosol–chemistry–climate model predictions and validation, J. Geophys. Res.-Atmos., 120, 256–276, doi:10.1002/2014JD021985, 2014. 4605, 4607

SPARC: Assessment of Stratospheric Aerosol Properties (ASAP), SPARC Report No. 4, edited by: Thomason, L. and Peter, T., World Climate Research Programme WCRP-124, WMO/TD No. 1295, 2006. 4603, 4604, 4607, 4609, 4611, 4613, 4614, 4621

Stenke, A., Schraner, M., Rozanov, E., Egorova, T., Luo, B., and Peter, T.: The SOCOL version 3.0 chemistry–climate model: description, evaluation, and implications from an advanced transport algorithm, Geosci. Model Dev., 6, 1407–1427, doi:10.5194/gmd-6-1407-2013, 2013. 4605, 4612

Stowe, L. L., Carey, R. M., and Pellegrino, P. P.: Monitoring the Mt. Pinatubo aerosol layer with NOAA/11 AVHRR data, Geophys. Res. Lett., 19, 159–162, doi:10.1029/91GL02958, 1992. 4602

Tabazadeh, A., Toon, O. B., Clegg, S. L., and Hamill, P.: A new parameterization of H_2SO_4/H_2O aerosol composition: atmospheric implications, Geophys. Res. Lett., 24, 1931–1934, doi:10.1029/97GL01879, 1997. 4605

Thomason, L. W., Poole, L. R., and Deshler, T.: A global climatology of stratospheric aerosol surface area density deduced from stratospheric aerosol and gas experiment II measurements: 1984–1994, J. Geophys. Res.-Atmos., 102, 8967–8976, doi:10.1029/96JD02962, 1997. 4603, 4608, 4609

Thomason, L. W., Burton, S. P., Luo, B.-P., and Peter, T.: SAGE II measurements of stratospheric aerosol properties at non-volcanic levels, Atmos. Chem. Phys., 8, 983–995, doi:10.5194/acp-8-983-2008, 2008. 4603, 4608

Timmreck, C., Graf, H.-F., and Feichter, J.: Simulation of Mt. Pinatubo volcanic aerosol with the Hamburg Climate Model ECHAM4, Theor. Appl. Climatol., 62, 85–108, doi:10.1007/s007040050076, 1999. 4603

Toohey, M., Krüger, K., Niemeier, U., and Timmreck, C.: The influence of eruption season on the global aerosol evolution and radiative impact of tropical volcanic eruptions, Atmos. Chem. Phys., 11, 12351–12367, doi:10.5194/acp-11-12351-2011, 2011. 4603

Weisenstein, D. K., Ko, M. K. W., Sze, N.-D., and Rodriguez, J. M.: Potential impact of SO_2 emissions from stratospheric aircraft on ozone, Geophys. Res. Lett., 23, 161–164, doi:10.1029/95GL03781, 1996. 4604

ACPD
15, 4601–4625, 2015

Weisenstein, D. K., Yue, G. K., Ko, M. K. W., Sze, N.-D., Rodriguez, J. M., and Scott, C. J.: A two-dimensional model of sulfur species and aerosols, J. Geophys. Res., 102, 13019–13035, doi:10.1029/97JD00901, 1997. 4603, 4604, 4605, 4612

Weisenstein, D. K., Penner, J. E., Herzog, M., and Liu, X.: Global 2-D intercomparison of sectional and modal aerosol modules, Atmos. Chem. Phys., 7, 2339–2355, doi:10.5194/acp-7-2339-2007, 2007. 4604, 4605

ACPD
15, 4601–4625, 2015

Table 1. Scores and rankings of 326 AER 2-D atmospheric simulations of the Pinatubo eruption sorted according to the weighted rank ("RankWt"). Scores of two additional 3-D simulations "R001 3-D" and "R149 3-D" from the aerosol-chemistry-climate model SOCOL-AER are provided at the bottom of the table.

Mass (Mt SO_2)	Location μ (km)	Scale σ (km)	Skewness α	Score SO_2	Score OPC	Score Burden	Score Ext	Score Avg	Score Wt	Rank SO_2	Rank OPC	Rank Burden	Rank Ext	Rank Avg	Rank Wt	Scenario Name
14	22.59	4	−2	0.22	0.47	0.16	0.25	0.28	0.25	20	23	7	11	2	1	R001
14	22.59	3	−2	0.11	0.47	0.19	0.28	0.27	0.26	4	24	14	28	1	2	
14	20.27	2	0	0.19	0.47	0.19	0.27	0.28	0.26	14	21	11	24	3	3	
14	21.43	3	−1	0.28	0.47	0.17	0.26	0.29	0.27	29	22	8	12	5	4	
14	21.43	4	−1	0.35	0.50	0.14	0.23	0.31	0.27	52	46	2	4	7	5	
14	19.11	3	0	0.38	0.48	0.15	0.24	0.31	0.27	57	32	4	7	9	6	
14	21.43	2	−1	0.19	0.45	0.21	0.30	0.29	0.28	13	13	19	43	4	7	
14	17.95	4	0	0.44	0.50	0.13	0.23	0.32	0.28	72	49	1	2	15	8	
14	20.27	3	0	0.31	0.53	0.17	0.24	0.31	0.28	42	67	9	6	8	9	
14	19.11	4	0	0.41	0.54	0.14	0.22	0.33	0.28	68	77	3	1	20	10	R010
14	22.59	3	−1	0.22	0.52	0.21	0.26	0.30	0.28	18	65	20	18	6	11	
14	22.59	4	−1	0.34	0.54	0.19	0.24	0.33	0.29	51	88	13	5	19	12	
14	20.27	4	−1	0.45	0.46	0.16	0.25	0.33	0.29	77	17	6	10	22	13	
14	21.43	4	−2	0.40	0.45	0.19	0.27	0.33	0.29	64	8	12	19	16	14	
14	16.79	4	0	0.50	0.48	0.15	0.24	0.34	0.29	88	29	5	8	27	15	
14	21.43	3	−2	0.37	0.44	0.21	0.28	0.32	0.30	54	3	18	33	14	16	
14	23.75	4	−2	0.29	0.54	0.22	0.26	0.33	0.30	36	81	24	15	18	17	
14	21.43	2	0	0.20	0.53	0.25	0.29	0.32	0.30	16	69	35	39	11	18	
14	21.43	2	−2	0.28	0.43	0.24	0.31	0.32	0.30	31	1	28	64	10	19	
14	17.95	3	0	0.51	0.46	0.18	0.26	0.35	0.31	89	16	10	16	32	20	
…	…	…														
14	23.75	3	−2	0.28	0.54	0.27	0.29	0.35	0.32	35	82	40	40	28	33	
17	22.59	4	−2	0.07	0.55	0.31	0.36	0.32	0.33	3	96	63	108	13	34	R034
17	21.43	4	−1	0.23	0.57	0.28	0.31	0.35	0.33	23	105	48	58	29	35	
…	…	…														
17	20.27	2	−2	0.63	0.50	0.34	0.37	0.46	0.43	120	45	89	119	94	93	
14	/	/	/	0.70	0.70	0.31	0.27	0.50	0.43	133	184	66	20	116	94	Box14Mt
20	17.95	2	0	0.61	0.53	0.35	0.37	0.46	0.43	112	68	92	112	95	95	
…	…	…														
14	26.07	3	−1	0.94	0.71	0.43	0.32	0.60	0.53	197	195	141	74	164	149	R149
…	…	…														
14	17.95	2	−2	0.96	0.61	0.56	0.57	0.67	0.64	207	133	207	227	208	215	
20	/	/	/	0.47	0.78	0.67	0.61	0.63	0.64	79	244	249	245	178	216	SPARC20Mt
14	16.79	2	−1	0.96	0.60	0.57	0.57	0.67	0.64	203	122	211	229	206	217	
…	…	…														
20	27.23	3	0	1.32	0.95	0.94	0.94	1.04	1.01	284	319	323	317	313	317	
20	29.55	4	0	1.35	0.95	0.94	0.95	1.05	1.01	293	318	319	324	316	318	
20	29.55	3	−2	1.47	0.91	0.91	0.94	1.06	1.01	308	308	309	316	318	319	
20	29.55	3	−1	1.46	0.92	0.92	0.95	1.06	1.02	307	310	313	322	320	320	
20	28.39	3	0	1.42	0.93	0.93	0.96	1.06	1.02	301	312	315	325	319	321	
20	29.55	2	0	1.68	0.85	0.86	0.94	1.08	1.02	323	281	291	319	324	322	
20	29.55	2	−2	1.68	0.86	0.87	0.94	1.09	1.03	322	284	295	315	325	323	
20	29.55	3	0	1.52	0.90	0.91	0.96	1.07	1.03	317	306	306	326	321	324	
20	28.39	2	0	1.60	0.88	0.89	0.95	1.08	1.03	320	298	298	323	322	325	
20	29.55	2	−1	1.67	0.86	0.88	0.95	1.09	1.03	321	288	297	321	326	326	
14	~ 22	4	−2	0.30	0.46	0.18	0.20	0.29	0.25							R001 3-D
14	~ 26	3	−1	0.93	0.53	0.36	0.38	0.55	0.49							R149 3-D

ACPD
15, 4601–4625, 2015

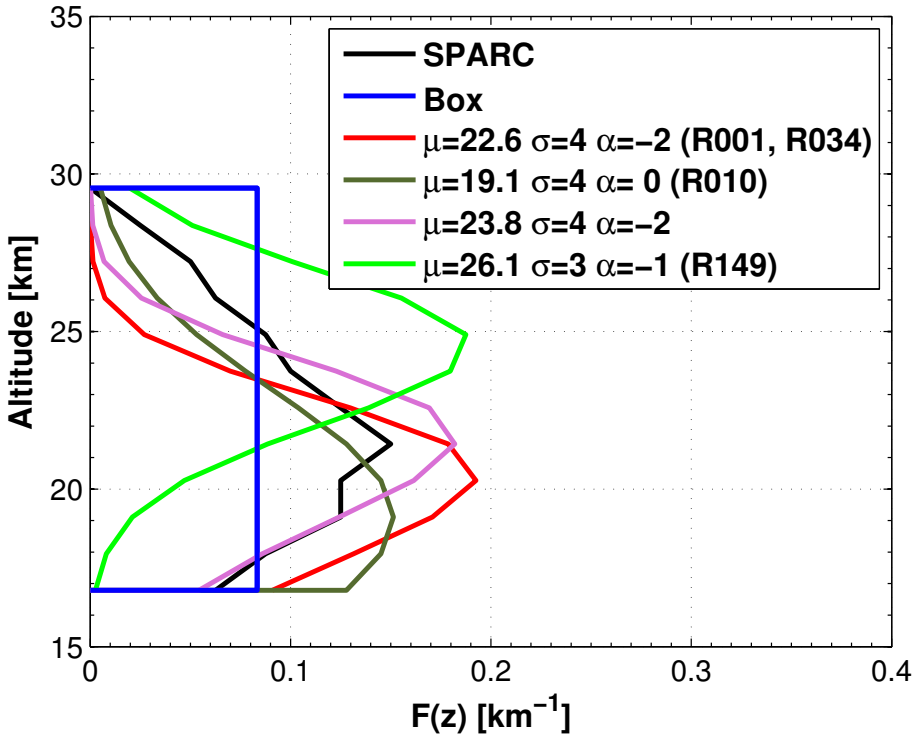

Figure 1. Vertical distribution function $F(z)$. Black line: used in SPARC (2006) Blue line: uniform (box) profile that distributes SO_2 homogeneously with altitudes. Each of these curves encloses a unit area.

ACPD
15, 4601–4625, 2015

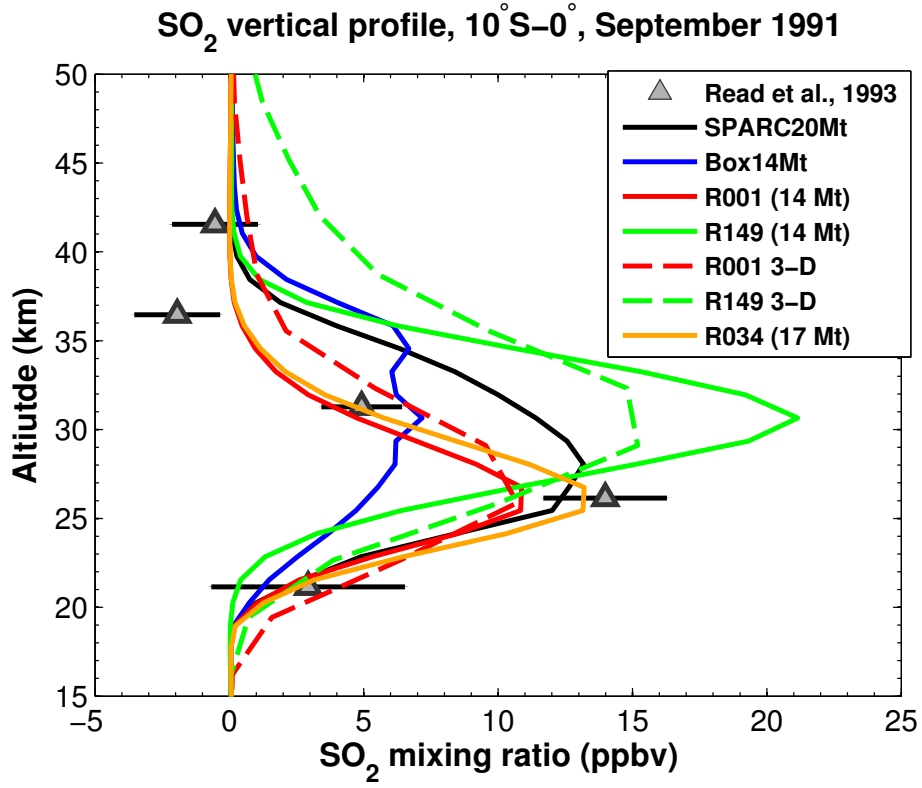

Figure 2. Vertical profiles of monthly zonal mean SO_2 mixing ratio at 10° S–0° N in September 1991. Simulations are represented in different colors. Observations (triangles) are taken from Microwave Limb Sounder (MLS) measurements (Read et al., 1993).

ACPD
15, 4601–4625, 2015

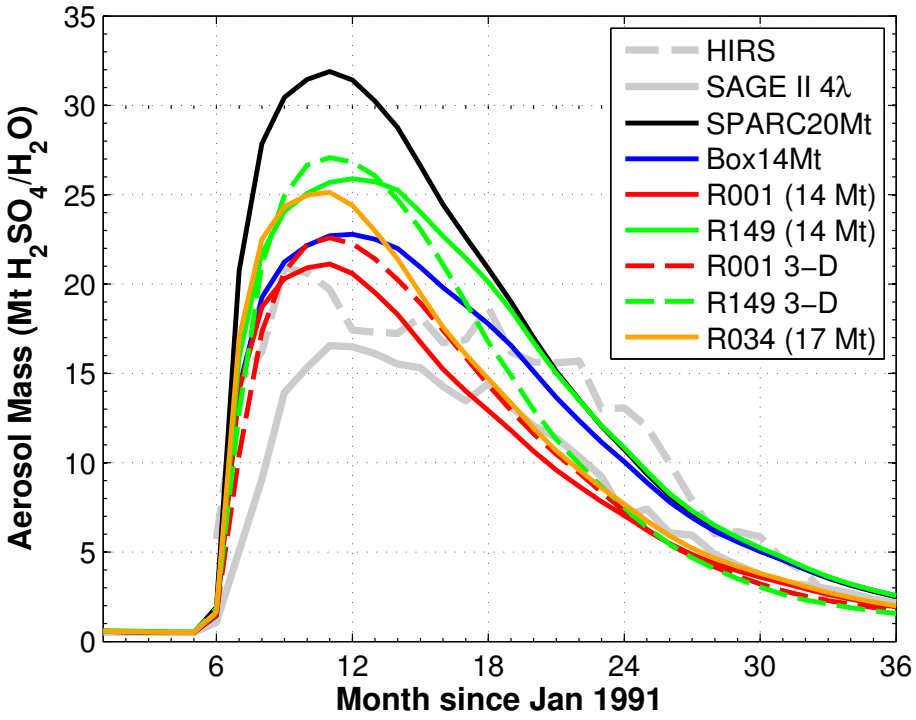

Figure 3. Evolution of simulated global stratospheric aerosol burden (Mt H_2SO_4/H_2O) compared to the HIRS and SAGE II-derived data. HIRS-derived data include both tropospheric and stratospheric aerosols (Baran and Foot, 1994). SAGE II aerosol data is derived from the retrieval algorithm SAGE 4λ by Arfeuille et al. (2013), and include only stratospheric aerosols.

ACPD
15, 4601–4625, 2015

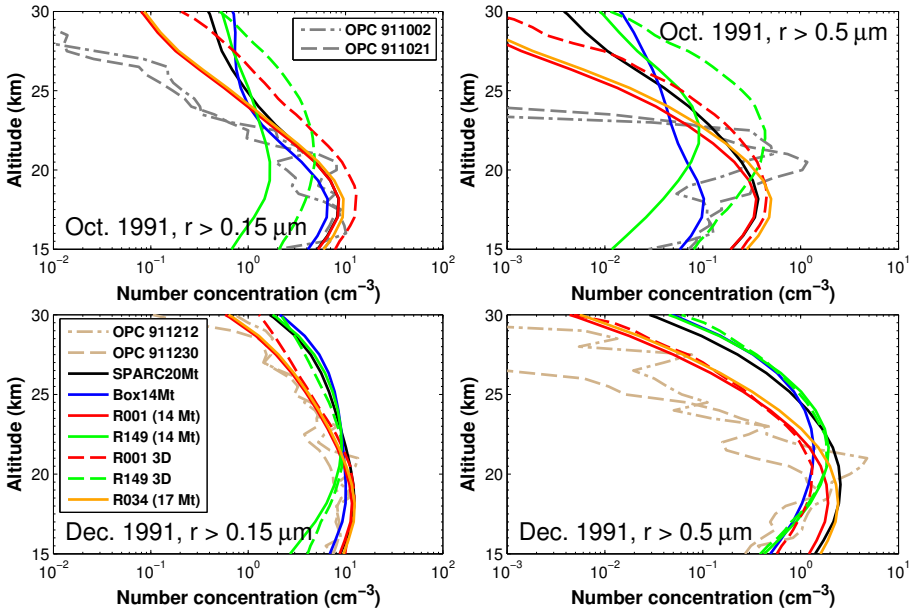

Figure 4. Cumulative particle number concentrations of OPC measurements (Deshler et al., 2003; Deshler, 2008), and model simulations in October 1991 (upper panels) and December 1991 (lower panels) for particle size channels $r > 0.15\,\mu m$ (left panels) and $r > 0.5\,\mu m$ (right panels).

ACPD
15, 4601–4625, 2015

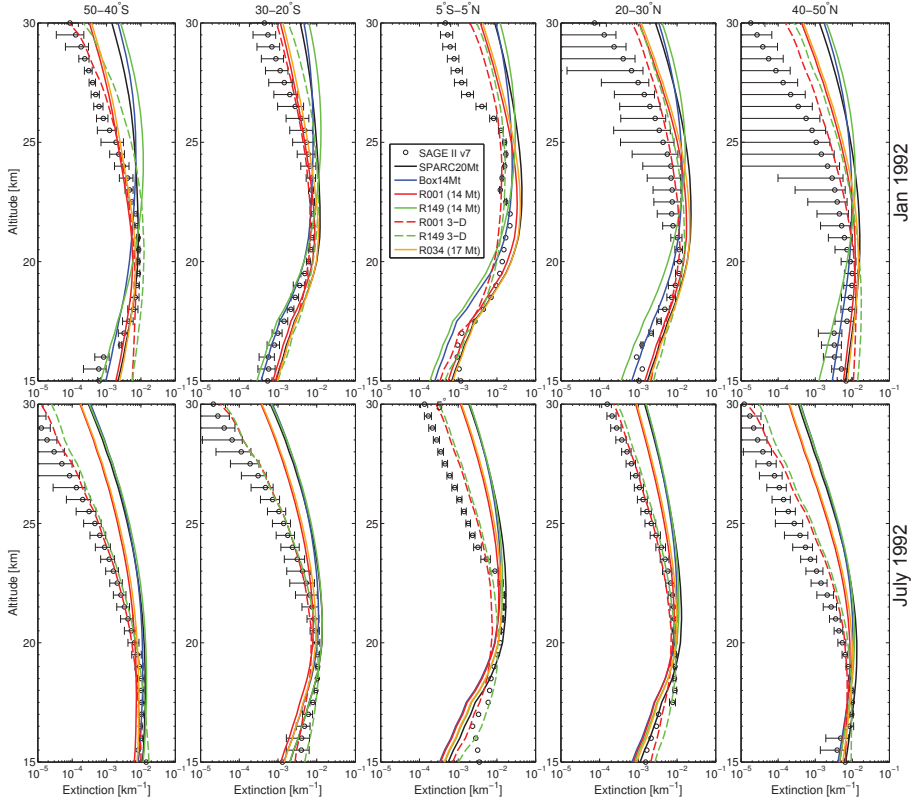

Figure 5. Aerosol 1020 nm extinction comparisons of SAGE II (version 7.0) and model simulations at five latitude bands 50–40° S, 30–20° S, 5° S–5° N, 20–30° N and 40–50° N for January (upper panel) and July 1992 (lower panel). Solid curves: AER 2-D model results. Dashed curves: 3-D SOCOL-AER model results.

ACPD
15, 4601–4625, 2015